

A New Soft-Switched DC-DC Front-End Converter for Applications with Wide-Range Input Voltage from Battery Power Sources

Yungtaek Jang and Milan M. Jovanović

Delta Products Corporation
Power Electronics Laboratory
P.O. Box 12173, 5101 Davis Drive
Research Triangle Park, NC 27709

Abstract — A technique which improves the performance of the two-inductor boost converter using a new active snubber circuit is described. The proposed snubber circuit consists of a small transformer, two diodes, and an auxiliary switch. This technique reduces reverse-recovery-related losses by controlling the di/dt rate of the rectifier current using a leakage inductance of the transformer. In addition, the energy stored in the leakage inductance is used to discharge the output capacitances of boost switches to zero voltage before they are turned on, thus eliminating their capacitive turn-on switching losses. Moreover, the reflected output voltage across the primary winding of the transformer resets the current in the leakage inductance and makes the auxiliary switch turn off using zero current switching. The performance of the proposed converter was evaluated on a 1.6-kW prototype circuit.

1. Introduction

Generally, telecommunication and computer networking industries use -48-V dc-bus distributed power systems, which are backed up by -48-V dc battery plants for their reliability, availability, and reserve time in case of ac outages. As a result, powering of power supplies using a -48-V dc bus and a universal ac-line is a common requirement for telecommunication and computer networking industries [1]. In fact, present specifications of power supplies for networking computer applications already call for designs with a universal ac-line input and a -48-V nominal dc input.

The requirement for dual input-voltage power supplies puts a significant burden on the power supply manufacturers because of the additional efforts and resources necessary to design, manufacture, and handle two versions of power supplies. Furthermore, since the quantity of the dc-input version is still a small fraction of the quantity of the ac-input version, the additional engineering effort required for the design of the dc-input version may not be profitable.

To minimize the effort and resources required for the design of power supplies which operate using dual input sources for networking computer applications, a modular design approach is a good choice. In this approach, the ac- and dc-input versions of power supplies use different front ends and the same output stage, as shown in Fig. 1. Specifically, the ac-input version employs a PFC boost-converter front end, whereas the dc-input version uses a dc-dc converter with a high input-to-output voltage gain. The

modular design does not require any redesign of the output stage since both front ends provide the same input voltage to the output stage, which is 380 V. Finally, the designs for both the ac and dc boost front ends can be standardized for a number of power levels. With standardized front-end modules, the design effort for dual-input power supplies can be dramatically reduced.

Recently, as shown in Fig. 2, a hard-switched two-inductor boost converter that is suitable for a dc-dc front-end converter of the modular design approach has been introduced in [2]. The hard-switched two-inductor boost converter employs auxiliary transformer ATR to achieve output-voltage regulation in wide load and input-voltage ranges with constant-frequency control. Moreover, the converter has a high voltage gain that is suitable for applications with a large difference between the input and output voltages. As shown in Fig. 2, by using a voltage-doubler rectifier, the output to input voltage gain is four times greater than that of the conventional boost converter topology.

However, since the converter shown in Fig. 2 operates with hard switching, reverse-recovery losses in output diodes and turn-on losses in boost switches limit its maximum switching frequency and conversion efficiency. So far, since many soft-switching techniques for a PFC boost-converter front end have been introduced in numerous papers [3]-[5], the efficiency of the ac-input version can be well optimized

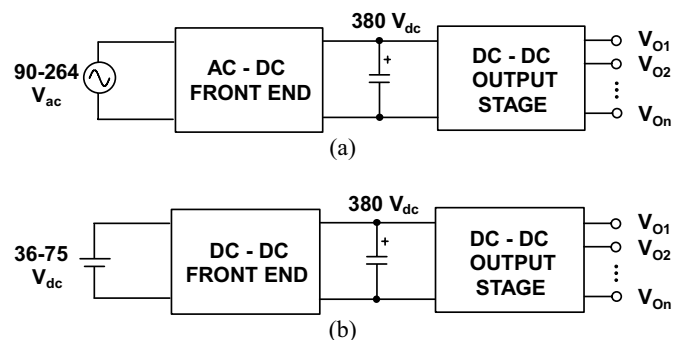
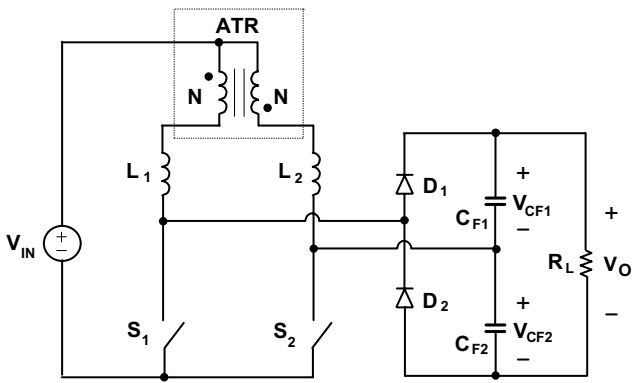
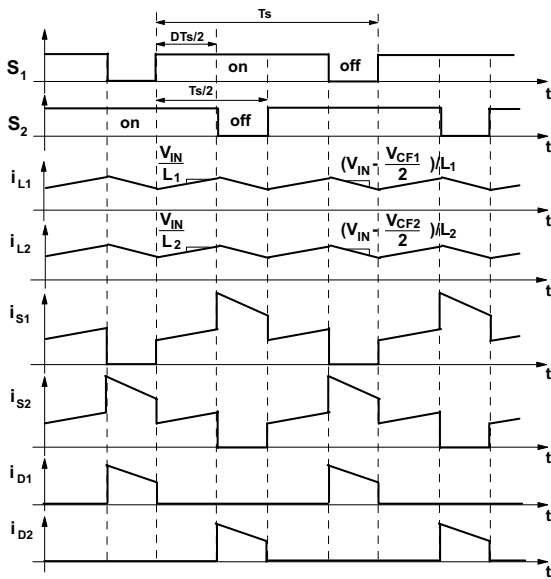


Fig. 1. Block diagrams of (a) ac-input version of power supply with PFC front end and (b) dc-input version of power supply with dc-dc front end.



(a)



(b)

Fig. 2. (a) Schematic diagram and (b) key waveforms of conventional hard-switched two-inductor boost converter with auxiliary transformer ATR.

by using one of the introduced techniques. Therefore, to maintain the overall efficiency of the dc-input version greater than or equal to the efficiency of the ac-input version, a suitable soft-switching technique for the converter in Fig. 2 is required.

In this paper, a technique which improves the performance of the two-inductor boost converter using a new active snubber circuit is introduced. As shown in Fig. 3, this technique reduces reverse-recovery-related losses by controlling the di/dt rates [6] of currents in diodes D_1 and D_2 utilizing a leakage inductance of the primary winding of transformer TR, which is connected in series with diodes D_3 and D_4 and auxiliary switch S_C . In addition, the energy stored in the leakage inductance is used to discharge the output capacitances of boost switches S_1 and S_2 to zero voltage

before they are turned on, thus eliminating their capacitive turn-on switching losses. Moreover, the reflected output voltage across the primary winding of transformer TR resets the current in the leakage inductance and makes auxiliary switch S_C turn off with zero current switching (ZCS).

The performance of the proposed soft-switched two-inductor boost converter with ATR was evaluated on a 1.6-kW prototype circuit that was designed to operate from a 36-60-V battery input and deliver up to 4.2 A at a 380 V output.

2. Brief Review of Conventional Two-Inductor Boost Converter with Auxiliary Transformer [2]

A non-isolated implementation of the two-inductor boost converter with auxiliary transformer ATR is shown in Fig. 2(a). The input side of the circuit consists of two switches S_1 and S_2 , two boost inductors L_1 and L_2 , and auxiliary transformer ATR. To maximize the voltage gain of the converter, the output side of the circuit is configured as a voltage doubler rectifier that consists of boost rectifiers D_1 and D_2 and output filter capacitors C_{F1} and C_{F2} connected across load R_L . As can be seen from the timing diagrams of the control signals for switches S_1 and S_2 shown in Fig. 2(b), switches S_1 and S_2 conduct simultaneously, i.e., they operate with overlapping control signals. The time of the simultaneous conduction, which is defined as the period from the turn-on moment of one switch until the turn-off moment of the other switch, represents duty cycle period $DTs/2$ of the converter.

It should be noted that because of the converter's unique property to simultaneously charge and discharge both boost inductors, which is due to the coupling of inductor currents through auxiliary transformer ATR, the converter can maintain the regulation of the output voltage with a constant frequency control in a wide range of the load current.

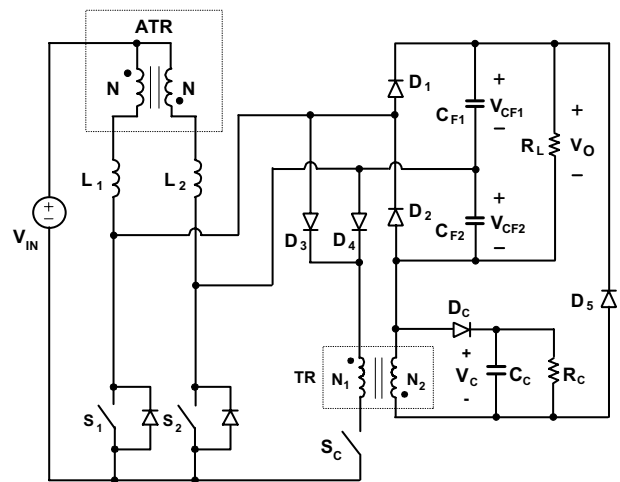


Fig. 3. Proposed soft-switched two-inductor boost converter with auxiliary transformer.

Namely, with the duty cycle close to unity, maximum power is transferred from the input to the output since the maximum amount of energy is stored in the inductors. As the duty cycle decreases toward zero, less and less energy is stored in both inductors, which enables the output voltage regulation down to very light loads. It also should be noted that if boost inductors L_1 and L_2 are equal, both inductors store and transfer the same amount of energy, i.e., each of the converter processes one half of the total power. Since the total power is processed in two parallel legs, the conduction loss of the circuit is small compared to a circuit with a single power path.

The voltage conversion ratio of the circuit can be calculated using the volt-second balance of the boost inductors. From Fig. 2(b), the volt-second balance equation for both boost inductors L_1 and L_2 is

$$V_{IN} D \frac{T_S}{2} = \left(\frac{V_{CF}}{2} - V_{IN} \right) \cdot (1-D) \cdot \frac{T_S}{2}, \quad (1)$$

so that

$$\frac{V_O}{V_{IN}} = \frac{4}{1-D}, \quad (2)$$

since $V_O = V_{CF1} + V_{CF2}$, where $V_{CF1} = V_{CF2} = V_{CF}$ and $L_1 = L_2 = L$. As can be seen from Eq. (2), the output voltage of the converter in Fig. 2 is at least four times larger than the input voltage. This high conversion ratio makes this converter very suitable for applications with a large difference between the output and input voltage.

3. Analysis of Proposed Soft-Switched Two-Inductor Boost Converter

The proposed soft-switched dc-dc front-end converter is shown in Fig. 3. The circuit consists of a conventional two-inductor boost converter with auxiliary transformer ATR and an additional soft-switching circuit which includes transformer TR, diodes D_3 and D_4 , and auxiliary switch S_C .

To facilitate the explanation of the circuit operation, Fig. 4 shows a simplified circuit diagram of the circuit in Fig. 3. In the simplified circuit, energy-storage capacitors C_{F1} and C_{F2} and reset capacitor C_C are modeled by voltage sources V_{CF1} , V_{CF2} , and V_C , respectively, assuming that the values of C_{F1} , C_{F2} , and C_C are large enough that the voltage ripples across the capacitors are small compared to their dc voltages. In addition, boost inductors L_1 and L_2 are modeled as constant current sources I_{L1} and I_{L2} by assuming that inductances L_1 and L_2 are large enough that, during a switching cycle, the currents through them do not change significantly. Because the turns ratio of ATR is unity and the magnetizing inductance of ATR is generally designed to be much larger than the boost inductances, boost inductor currents I_{L1} and I_{L2} can be assumed equal and the same as one half of input current I_{IN} [2]. Also, transformer TR is modeled by leakage inductance L_{LK} , magnetizing inductance L_M , and an ideal transformer with turns ratio $n = N_1/N_2$. Finally, it is assumed

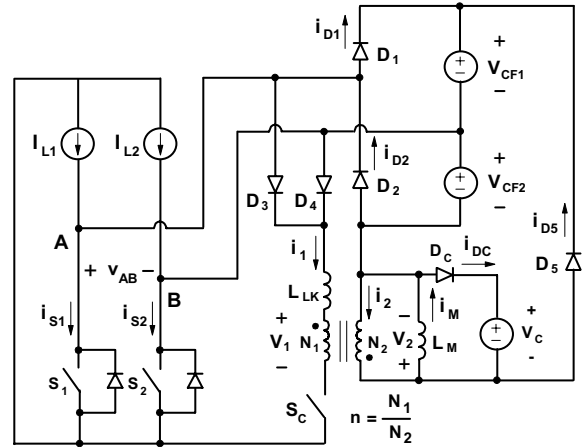


Fig. 4. Simplified circuit model of proposed converter that shows reference directions of currents and voltages.

that in the on state, semiconductors exhibit zero resistance, i.e., they are short circuits. However, the output capacitance of the switches, as well as the junction capacitance and the reverse-recovery charge of the rectifier, is not neglected in this analysis.

To further facilitate the analysis of operation, Fig. 5 shows the topological stages of the circuit in Fig. 3 during a switching cycle, whereas Fig. 6 shows its key waveforms. The reference directions of currents and voltages plotted in Fig. 6 are shown in Fig. 4.

As can be seen from the timing diagram of the drive signals for switches S_1 , S_2 , and S_C shown in Fig. 6, auxiliary switch S_C is turned on prior to the turn on of boost switches S_1 and S_2 . However, switch S_C is turned off before boost switches S_1 and S_2 are turned off.

Prior to the turn on of switch S_C at $t=T_0$, switches S_1 and S_C are open, and inductor current I_{L1} flows through boost rectifier D_1 into voltage source V_{CF1} . During this period, switch S_2 is closed, and both inductor currents I_{L1} and I_{L2} flow through S_2 , as shown in Fig. 6. After switch S_C is turned on at $t=T_0$, current I_{L1} starts flowing through primary winding N_1 of transformer TR and induces current i_2 in secondary winding N_2 , as shown in Fig. 5(a). Because during this stage output voltage V_O , which is equal to the sum of voltages V_{CF1} and V_{CF2} , is impressed across winding N_2 , transformer winding voltages v_1 and v_2 are given by

$$v_2 = V_O \quad \text{and} \quad (3)$$

$$v_1 = \frac{N_1}{N_2} V_O = nV_O, \quad (4)$$

where it is required that $n = N_1/N_2 < 0.5$ for the proper operation of the circuit. Since v_1 is constant, voltage applied across leakage inductance L_{LK} of the transformer is also constant so that current i_1 increases linearly with a slope of

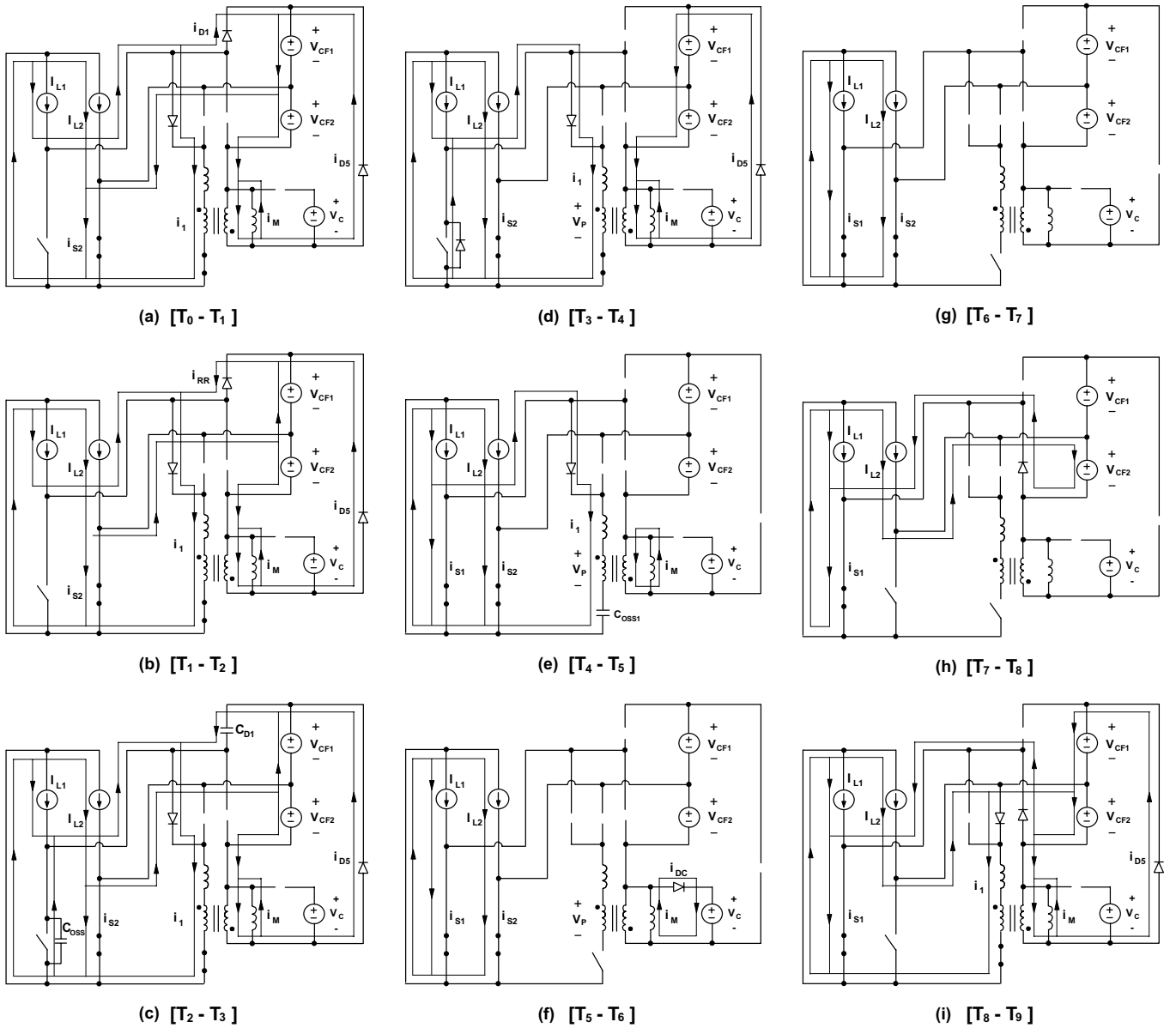


Fig. 5. Topological stages of proposed converter.

$$\frac{di_1}{dt} = \frac{V_O - v_1}{L_{LK}} = \frac{V_O - nV_O}{L_{LK}} = \left(\frac{1}{2} - n\right) \frac{V_O}{L_{LK}}. \quad (5)$$

At the same time, magnetizing inductance i_M also increases with a slope given by

$$\frac{di_M}{dt} = \frac{V_O}{L_M}. \quad (6)$$

As current i_1 linearly increases, boost rectifier current i_{D1} linearly decreases at the same rate since the sum of i_1 and i_{D1} is equal to constant inductor current I_{L1} , i.e. $i_1 + i_{D1} = I_{L1}$. Therefore, in the proposed circuit, the turn-off rate of the boost rectifier

$$\frac{di_{D1}}{dt} = \left(n - \frac{1}{2}\right) \frac{V_O}{L_{LK}} \quad (7)$$

can be controlled by a proper design of transformer TR, specifically by the value of its leakage inductance L_{LK} and turns ratio n . Typically, for today's fast-recovery rectifiers, the turn-off rate, di_D/dt , should be kept around 100 A/ μ s.

The topological stage in Fig. 5(a) ends at $t=T_1$, when boost rectifier current i_{D1} falls to zero. Due to a stored charge in the rectifier, the rectifier current continues to flow in a negative direction, as shown in Figs. 5(b) and 6. Generally, for properly selected leakage inductance L_{LK} and turns ratio n , this reverse-recovery current is substantially reduced compared to the corresponding current in a circuit without

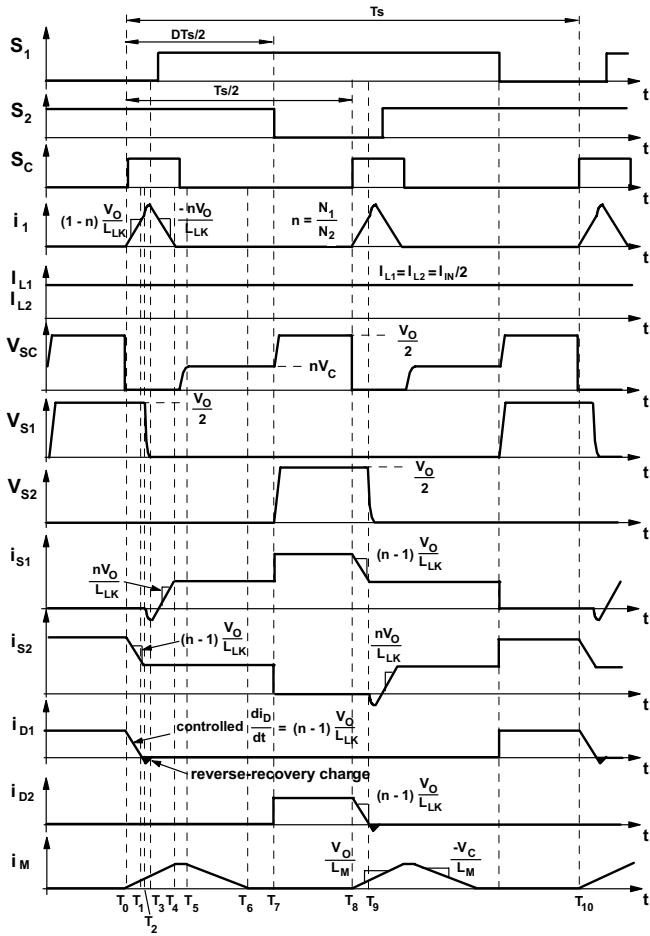


Fig. 6. Key waveforms of proposed converter.

the boost rectifier turn-off di/dt rate control. After the stored charge is removed from the rectifier, which occurs at $t=T_2$ in Fig. 6, the rectifier regains its voltage blocking capability and the circuit enters the topological stage shown in Fig. 5(c). During this stage, junction capacitance C_{D1} of boost rectifier D_1 is charged and output capacitance C_{OSS} of boost switch S_1 is discharged through a resonance between the parallel connection of C_{D1} and C_{OSS} with leakage inductance L_{LK} . The expressions for boost-switch voltage v_{S1} and leakage-inductor current i_1 during this resonance are

$$i_1 = I_{IN} + I_{RR(PK)} + \frac{(\frac{1}{2} - n)V_O}{Z_C} \sin(\omega_R t) \quad (8)$$

and

$$v_{S1} = \frac{V_O}{2} - \left(\frac{1}{2} - n\right)V_O(1 - \cos(\omega_R t)), \quad (9)$$

where characteristic impedance Z_C and resonant angular frequency ω_R are defined as

$$Z_C = \sqrt{\frac{L_{LK}}{C_{OSS} + C_{D1}}} \quad (10)$$

$$\omega_R = \frac{1}{\sqrt{L_{LK}(C_{OSS} + C_{D1})}}, \text{ respectively.} \quad (11)$$

From Eq. (9), it can be seen that to completely discharge output capacitance C_{OSS} of boost switch S_1 and, therefore, create the condition needed for the zero-voltage turn on of switch S_1 , it is necessary that at the end of the resonance at $t=T_3$

$$v_{S1}(t=T_3) = \frac{V_O}{2} - \left(\frac{1}{2} - n\right)V_O(1 - \cos \pi) = 0, \quad (12)$$

which limits maximum turns ratio n_{MAX} of transformer TR to $n_{MAX} = 0.25$.

If turns ratio $n < 0.25$ is selected, output capacitance C_{OSS} of boost switch S_1 can always be discharged to zero regardless of the load and line conditions. Once the capacitance is fully discharged at $t=T_3$, current i_1 continues to flow through the antiparallel diode of boost switch S_1 , as shown in Fig. 5(d). Because, during this topological stage, voltage v_1 is impressed in a negative direction across leakage inductance L_{LK} , current i_1 begins to linearly decrease at the rate given by

$$\frac{di_1}{dt} = -\frac{nV_O}{L_{LK}}, \quad (14)$$

as illustrated in Figs. 5(d) and 6. As a result, auxiliary-switch current i_1 also starts linearly decreasing, whereas boost-switch current i_{S1} starts linearly increasing from a negative peak, as shown in Fig. 6. To achieve zero-voltage switching (ZVS) of boost switch S_1 , it is necessary to turn on boost switch S_1 before its current becomes positive, i.e., until i_{S1} still flows through the antiparallel diode of switch S_1 .

With boost switch S_1 turned on shortly after $t=T_3$, boost-switch current i_{S1} continues to flow through closed switch S_1 after it becomes positive, as shown in Fig. 6. In this topological stage, current i_1 continues to decrease linearly toward zero, while boost-switch current i_{S1} continues to linearly increase at the same rate. When current i_1 becomes zero at $t=T_4$, boost-switch current i_{S1} reaches I_{L1} so that the entire inductor current I_{L1} flows through boost switch S_1 , as shown in Fig. 6. At the same time, auxiliary switch S_C carries no current so that auxiliary switch S_C can be turned off with zero current.

When auxiliary switch S_C is turned off with ZCS shortly after $t=T_4$, magnetizing current i_M begins to charge output capacitance C_{OSS1} of auxiliary switch S_C , as shown in Fig. 5(e). When voltage v_{SC} across auxiliary switch S_C reaches reset voltage nV_C at $t=T_5$, where V_C is the voltage across reset capacitor C_C , magnetizing current i_M is commutated into the voltage source V_C , which models the reset circuit. As shown in Fig. 5(f), during this stage, negative voltage V_C resets the magnetizing current with a rate

$$\frac{di_M}{dt} = -\frac{V_C}{L_M} \quad (15)$$

until magnetizing current i_M becomes zero at $t=T_6$.

After transformer TR is reset at $t=T_6$, the circuit stays in the topological stage shown in Fig. 5(g) until boost switch S_2 is open at $t=T_7$ and inductor current I_{L2} is commutated from switch S_2 to its output capacitance C_{OSS} . Due to C_{OSS} charging with constant current I_{L2} , voltage v_{S2} will increase linearly until it reaches V_{CF2} , and inductor current I_{L2} is instantaneously commutated to boost rectifier, as shown in Figs. 5(h) and 6. The circuit stays in the topological stage in Fig. 5(h) until $t=T_8$, which is when auxiliary switch S_C is turned on again. After switch S_C is turned on at $t=T_8$, current I_{L2} starts flowing through primary winding N_1 of transformer TR and induces current i_2 in secondary winding N_2 , as shown in Fig. 5(i). The topological stages during the time between $t=T_9$ and $t=T_{10}$ are similar to the topological stages during the time between $t=T_1$ and $t=T_8$. The roles of boost switches S_1 and S_2 are switched during this period.

In summary, the major feature of the proposed circuit is the soft-switching of all semiconductor devices. Boost switches S_1 and S_2 are turned on with ZVS, auxiliary switch S_C is turned off with ZCS, and boost diodes D_1 and D_2 are turned off with a controlled di/dt rate. As a result, the turn-on switching loss in the boost switches, the turn-off switching loss in the auxiliary switch, and reverse-recovery-related losses in the boost rectifiers are eliminated, which minimizes the overall switching losses and, therefore, maximizes the conversion efficiency. In addition, soft-switching has beneficial effect on EMI, which may result in a smaller size of the input filter.

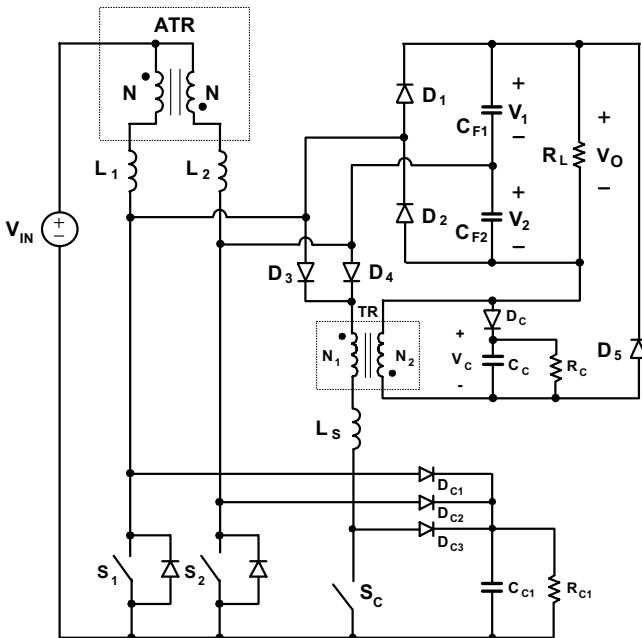


Fig. 7. Proposed soft-switched two-inductor boost converter with external snubber inductor L_S and the clamp circuit that prevents an accidental simultaneous opening of both boost switches S_1 and S_2 .

The leakage inductance of transformer TR is determined from the desired turn-off di/dt rate of the boost rectifier current defined in Eq. (7), i.e.,

$$L_{LK} = \frac{\left(\frac{1}{2} - n\right)V_O}{di_D/dt}. \quad (16)$$

As can be seen from Eq. (16), to minimize the value of leakage inductance L_{LK} , it is desirable to maximize turns ratio n of the transformer. Since $n_{MAX}=0.25$, the turns ratio of the transformer should not be much less than 0.25. Typically, the values of n that are in the 0.1-0.25 range are optimal. Assuming that $V_O=400$ V, $n=0.25$, and $di_D/dt=100$ A/ μ s, the leakage inductance value of $L_{LK}=1$ μ H is obtained. If this inductance is too large to be the leakage inductance of the transformer, external snubber inductor L_S can be used to adjust the desired circuit inductance as shown in Fig. 7.

4. Experimental Results

The performance of the proposed soft-switched two-inductor boost converter was evaluated on a 1.6-kW prototype circuit that was designed to operate from a 36-V–60-V battery input and deliver up to 4.2 A at a 380 V output. Switches S_1 and S_2 both operate at 150 kHz while auxiliary switch S_C operates at 300 kHz.

Since the drain voltages of switches S_1 and S_2 are clamped to output capacitors C_{F1} and C_{F2} , respectively, the peak voltage stress on switches S_1 and S_2 is approximately 190 V. The peak current stress on switches S_1 and S_2 , which occurs at full load and low line, is approximately 50 A. Therefore, three IRFP264 MOSFETs ($V_{DSS} = 250$ V, $I_{D25} = 38$ A, $R_{DS} = 0.075$ Ω) from IR that were connected in parallel were used for each of the switches. Moreover, a high speed HGTG12N60A4 IGBT ($V_{RRM} = 600$ V, $I_F = 12$ A) from Fairchild was used as auxiliary switch S_C .

Since output diodes D_1 and D_2 must block the output voltage and must conduct the peak load current which is approximately 4.2 A, two RHRP3060 diodes ($V_{RRM} = 600$ V, $I_{FAVM} = 30$ A) from Fairchild were used as output diodes D_1 and D_2 . Two RHRP1560 diodes ($V_{RRM} = 600$ V, $I_{FAVM} = 15$ A) were used as diodes D_3 and D_4 . An RHRP860 diode ($V_{RRM} = 600$ V, $I_{FAVM} = 8$ A) was used as diode D_5 . To reduce the conduction losses of the switches and output diodes, devices which have higher current ratings than the designed maximum current were selected.

To obtain the desired inductance of boost inductors L_1 and L_2 of approximately $L_1=L_2=L=12$ μ H at full load, each boost inductor was built using a toroidal core (Magnetics, Kool- μ 77552-A7) and 30 turns of magnet wire (AWG #14). A ferrite toroidal core (Philips, Ferrite TX29/19/7.6) was used in parallel with a Kool- μ core to increase the continuous-conduction-mode operation boundary. Specifically, a Kool- μ core and a ferrite toroidal core were wound together using magnet wire.

External snubber inductor L_S was connected in series with the primary winding of transformer TR, as shown in Fig. 7. The required inductance is approximately $1.4 \mu\text{H}$ at full load. Snubber inductor L_S was built using a toroidal core (MPP, A189043) from Arnold and 6 turns of magnet wire (AWG #18).

Auxiliary transformer ATR was built using a pair of ferrite cores (Philips, ER28L-3F3) with an air gap (2 mils). Two AWG #14 magnet wires with equal number of turns (11 turns:11 turns) were used to obtain a desired magnetizing inductance, which is approximately $100 \mu\text{H}$. Transformer TR was built using a ferrite toroidal core (T25/15/13) with two windings ($N_1=5$ turns: $N_2=40$ turns).

Two aluminum capacitors ($1500 \mu\text{F}$, 250 VDC) were used for output capacitors C_{F1} and C_{F2} . Both capacitors have an equal voltage stress which is a half of output voltage V_O , since the proposed converter naturally balances the voltages of output capacitors C_{F1} and C_{F2} .

It should be noted that an accidental simultaneous opening of both switches would lead to a catastrophic circuit failure since the energy stored in the boost inductors would not have a path to discharge. Therefore, to prevent the circuit failure, it

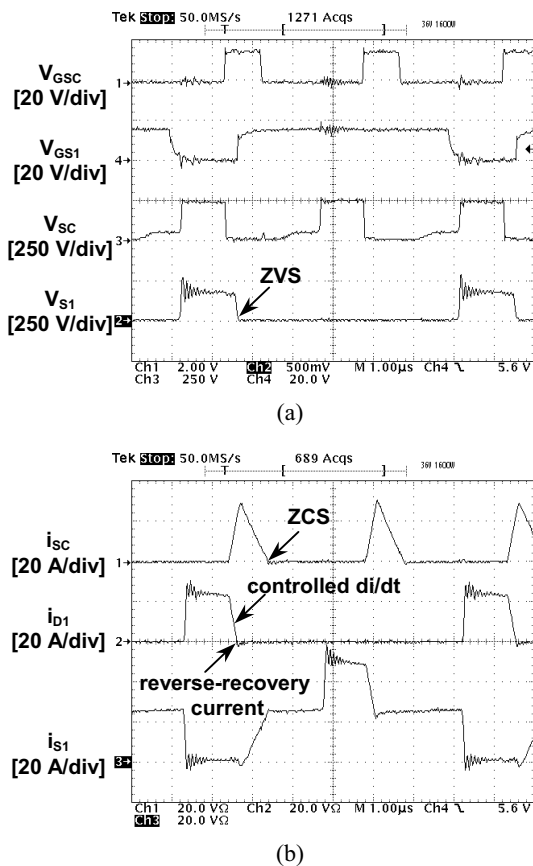


Fig. 8. Measured key waveforms of experimental converter at $P_o = 1600 \text{ W}$ and $V_{IN} = 36 \text{ V}$. Time base: $1 \mu\text{s}/\text{div}$.

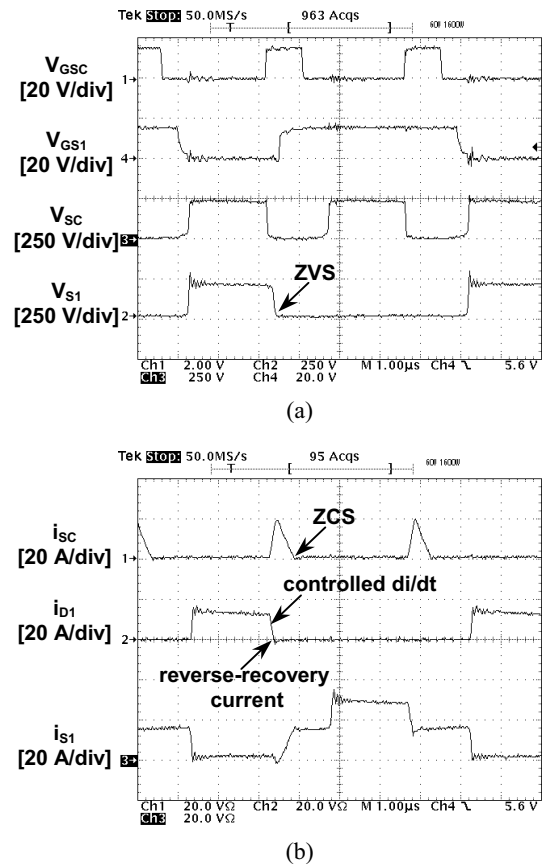


Fig. 9. Measured key waveforms of experimental converter at $P_o = 1600 \text{ W}$ and $V_{IN} = 60 \text{ V}$. Time base: $1 \mu\text{s}/\text{div}$.

is necessary to provide a discharging path for the energy of the boost inductors when both switches are open. Figure 7 shows a protection circuit implemented with a RCD snubber connected across the switches. The clamp circuit consists of three diodes D_{C1} , D_{C2} , and D_{C3} , capacitor C_{C1} , and resistor R_{C1} . An aluminum capacitor ($25 \mu\text{F}$, 250 VDC) was used for clamp capacitor C_{C1} and a carbon resistor ($43 \text{ k}\Omega/2 \text{ W}$) was used for clamp resistor R_{C1} . Three fast diodes (BYV-26C) were used for D_{C1} , D_{C2} , and D_{C3} .

Finally, the reset circuit for transformer TR consists of diodes D_C , reset capacitor C_C , and resistor R_C . A polyester capacitor ($0.47 \mu\text{F}$, 250 VDC) was used for reset capacitor C_C and a carbon resistor ($10 \text{ k}\Omega/2 \text{ W}$) was used for resistor R_C . A fast diode (BYV-26C) was used for diode D_C .

Figures 8 and 9 show the oscillograms of key waveforms in the experimental converter, when it delivers full power from the low line and high line input voltages, respectively. As can be seen from the corresponding waveforms in Fig. 6, there is a good agreement between the experimental and theoretical waveforms. As can be seen from Figs. 8(a) and 9(a), switches S_1 and S_2 (MOSFETs) are turned on with ZVS since their voltages V_{S1} and V_{S2} fall to zero before gate-drive signals V_{GS1} and V_{GS2} become high. Moreover, auxiliary

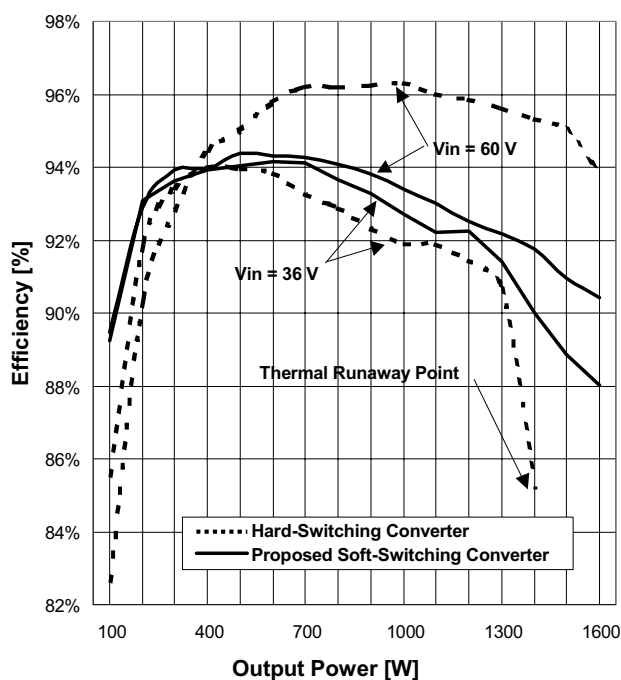


Fig. 10. Measured efficiencies of the 150-kHz, 1.6-kW experimental converter with (dashed lines) hard switching and (solid lines) soft switching at $V_{IN} = 36$ V and $V_{IN} = 60$ V as functions representing output power. Note that the maximum possible output power of the hard-switching two-inductor boost converter is limited to 1.3 kW.

switch S_C achieves soft-switching turn off because switch current i_{SC} becomes zero before auxiliary switch S_C is turned off, as shown in Figs. 8(b) and 9(b). Also, it should be noted that the slope of rectifier current i_{D1} is approximately $di/dt = 100$ A/ μ s during the period when diode D_1 is turned off. The rectifier-current slope is controlled by snubber inductance L_S , as indicated in Figs. 8(b) and 9(b). With this di/dt rate, peak reverse-recovery current I_{RR} is reduced to approximately 2 A.

Figure 10 shows the measured efficiencies of the experimental converter with (solid lines) and without (dashed lines) the active snubber circuit at the minimum and maximum line voltages as functions representing output power. As can be seen in Fig. 10, for a low line voltage, the active snubber improves the conversion efficiency in the entire measured power range (100 W to 1.6 kW). The efficiency improvement is pronounced at the minimum line and higher power levels where the reverse-recovery losses are greater. At the minimum line, the active snubber improves the efficiency by approximately 0.7% at 1.3 kW, which translates into approximately 10% reduction of losses.

Furthermore, at the same power levels, the temperatures of the semiconductor components in the implementation with the active snubber are significantly lower than those in the implementation without the snubber. At the minimum line and 1.3 kW output power, the case temperatures of the boost

switches and boost rectifiers in the implementation with the snubber are $T_S = 62^\circ\text{C}$ and $T_d = 49^\circ\text{C}$, respectively, at an ambient temperature of $T_a = 27^\circ\text{C}$, whereas the corresponding temperatures in the implementation without the snubber are $T_S = 82^\circ\text{C}$ and $T_d = 74^\circ\text{C}$ at the same ambient temperature. As can be seen from Fig. 10, the implementation without the snubber cannot deliver the full power of 1.6 kW at the minimum line because the switches may become thermally unstable at a higher ambient temperature.

Since all switches operate with zero-voltage or zero-current switching, the rectifier reduces switching losses and thereby improves the spectral performance of the rectifier for less EMI.

5. Summary

A new soft-switched two-inductor boost converter with an auxiliary transformer that can achieve soft-switching of all semiconductor devices has been described. Boost switches S_1 and S_2 are turned on with ZVS, auxiliary switch S_C is turned off with ZCS, and boost diodes D_1 and D_2 are turned off with a controlled di/dt rate. As a result, the turn-on switching loss in the boost switches, the turn-off switching loss in the auxiliary switch, and reverse-recovery-related losses in the boost rectifiers are eliminated, which maximizes the conversion efficiency. The performance of the proposed converter was verified on a 1.6-kW prototype circuit that was designed to operate from a 36-60-V battery input and deliver up to 4.2 A at a 380-V output.

References

- [1] J. Akerlund, "-48 V DC computer equipment topology – an emerging technology," *IEEE International Telecommunications Energy Conf. (INTELEC) Proc.*, pp. 15-21, Oct. 1998.
- [2] Y. Jang and M. M. Jovanović, "New Two-Inductor Boost Converter with Auxiliary Transformer," *IEEE Applied Power Electronics Conf. Rec.*, pp. 654 - 660, 2002.
- [3] G. Hua, X. Yang, Y. Jiang, F.C. Lee, "Novel zero-current-transition PWM converters," *IEEE Power Electronics Specialists' Conf. (PESC) Rec.*, pp. 538 - 544, June 1993.
- [4] K. Wang, G. Hua, F.C. Lee, "Analysis, design and experimental results of ZCS-PWM Boost Converters," *International Power Electronics Conf. Proc.*, pp. 1202-1207, Yokohama, Japan, April 1995.
- [5] Y. Jang and M. M. Jovanović, "A New, Soft-Switched, High-Power-Factor Boost Converter with IGBTs," *IEEE International Telecommunications Energy Conf. (INTELEC) Proc.*, 8-3, June 1999.
- [6] Y. Khersonsky, M. Robinson, D. Gutierrez, "New fast recovery diode technology cuts circuit losses, improves reliability," *Power Conversion & Intelligent Motion (PCIM) Magazine*, pp. 16 - 25, May 1992.